Millennial meridional dynamics of Indo-Pacific Warm Pool during the last termination

Li Lo[1], Chuan-Chou Shen[1,*], Kuo-Yen Wei[1], George S. Burr[1,2], Horng-Sheng Mii[3], Min-Te Chen[4], Shih-Yu Lee[5], Meng-Chieh Tsai[1]

[1]High-Precision Mass Spectrometry and Environment Change Laboratory (HISPEC), Department of Geosciences, National Taiwan University, Taipei 10617, Taiwan ROC

[2]NSF-Arizona Accelerator Mass Spectrometry Facility, Department of Physics, University of Arizona, Tucson, AZ 85721, USA

[3]Department of Earth Sciences, National Taiwan Normal University, Taipei 11677, Taiwan ROC

[4]Institute of Applied Geosciences, National Taiwan Ocean University, Keelung 20224, Taiwan ROC

[5]Research Center for Environmental Changes, Academia Sinica, Taipei 11529, Taiwan ROC

Revised to *Climate of the Past*

2014.11.30

*Corresponding Author: Chuan-Chou Shen

Email: river@ntu.edu.tw; Tel: 886-2-3366-5878; Fax: 886-2-3365-1917

Abstract

To develop an in-depth understanding of the natural dynamics of the Indo-Pacific Warm Pool (IPWP) during the last deglaciation, stacked North- (N-) and South-IPWP (S-IPWP) thermal and hydrological records over the past 23-10.5 thousand years (ka) were built using planktonic foraminiferal geochemistry data from a new core, MD05-2925 (9.3^{o}S, 151.5^{o}E, water depth 1661 m) in the Solomon Sea and eleven previous sites. Ice-volume corrected seawater $\delta^{18}O$ ($\delta^{18}O_{SW\text{-}IVC}$) stacks show that S-IPWP $\delta^{18}O_{SW\text{-}IVC}$ values are indistinguishable from their northern counterpart through glacial time. The N-IPWP SST stacked record features an increasing trend of 0.5 ^{o}Cka^{-1} since 18 ka. Its S-IPWP counterpart shows an earlier onset of temperature increase at 19 ka and a strong teleconnection to high-latitude climate in the Southern Hemisphere. Meridional SST gradients between N- and S-IPWP were 1 to 1.5 ^{o}C during the Bølling/Allerød period and 1 ^{o}C during both Heinrich event 1 and the Younger Dryas due to a warmer S-IPWP. A warm S-IPWP during the cold events may possibly weaken the southern hemispheric branch of the Hadley Cell and reduce precipitation in the Asian Monsoon region.

1. Introduction

The Indo-Pacific Warm Pool (IPWP) is the largest warm water mass in the world, with an annual average sea surface temperature (SST) greater than 28 ^{o}C (Yan et al., 1992). Vigorous regional atmosphere circulation transports latent heat and water moisture from the IPWP to the middle and high latitudes (Yan et al., 1992). For the past five decades, the IPWP has experienced surface water freshening and a westward shift in precipitation, resulting in regional drought in East Africa and storm track changes in East Australia (Cravatte et al., 2009; Williams and Funk, 2011). Since the early 2000s, intensive paleoclimatological studies have been conducted to understand long-term thermal and hydrological changes in the IPWP, associated with glacial/interglacial (G/IG) cycles, and to constrain the relationship between warm pool thermal and hydrological fluctuations to high latitude ice sheet and greenhouse gas concentrations during the late Pleistocene (e.g., Lea et al., 2000; Stott et al., 2002; Visser et al., 2003; Rosenthal et al., 2003; Stott et al., 2004; de Garidel-Thoron et al., 2005; Steinke et al., 2006; Levi et al., 2007; Xu et al., 2008; Linsley et al., 2010; Bolliet et al., 2011; Mothadi et al., 2014).

Stacked IPWP SST and seawater oxygen isotope ($\delta^{18}O_{SW}$) records from the last glacial to the Holocene clearly show a close link between the IPWP SST, the Asian-Australian Monsoon (AAM) system, and sea level (Stott et al., 2004; Oppo et al., 2009; Linsley et al., 2010). However, a complicated ocean-island configuration and regional topography hinder the fidelity of using these records to describe past climate changes in detail (Griffiths et al., 2009; Mohtadi et al., 2011). In particular, little is known about the meridional

thermal-hydrological dynamics between the N-IPWP and S-IPWP during the last termination.

Here we present new oceanic proxy-inferred SST and ice volume-corrected surface seawater oxygen isotope $\delta^{18}O$ ($\delta^{18}O_{SW\text{-}IVC}$) records from the Solomon Sea, Papua New Guinea (PNG) for the past 23-10.5 thousand years ago (ka, before 1950 AD, hereafter). New SST and $\delta^{18}O_{SW\text{-}IVC}$ stacked records since the last termination are built for both the N- and S-IPWP to understand regional thermal-hydrological changes and interhemispheric teleconnections.

2. Material and Methods

Site MD05-2925 (9.3°S, 151.5°E, water depth 1661 m) is located at the northern slope of the Woodlark Basin in the Solomon Sea, which is the passage of surface and subsurface water masses between low- and middle-latitude South Pacific Ocean gyre and cross equatorial currents (Grenier et al., 2011; Melet et al., 2011) (Fig. 1). The seasonal precipitation in this region (Fig. 1) is dominated by the AAM system, coupled with the intertropical convergence zone (ITCZ) (Shiau et al., 2012, and references therein). Tests of single species planktonic foraminifera, *Globigerinoides sacculifer* (> 500 μm, total amount of 2-6 mg), at 13 selected depths were picked for accelerator mass spectrometry (AMS) ^{14}C dating. The AMS dates were calibrated using the CALIB 6.0.1 program (Stuiver et al., 2010, Table 1; Reimer et al., 2009) to reconstruct an age model for a time interval from 23 to 10.5 ka.

Forty to sixty individuals of the planktonic foraminifera *Globigerinoides ruber* (white, *s.s.*, 250-300 μm) were picked under the microscope. For Mg/Ca measurements, 20-30 individuals were gently crushed and transported into a

1.5 mL Teflon vial. The cleaning procedure was as follows: (1) foraminiferal fragments were immersed in ethanol, (2) a 0.45 mL aliquot of 3% H_2O_2, (3) NH_4Cl (0.45 mL, 1.0 N), (4) NH_2OH (0.45 mL, 0.01 N), and then (5) dilute nitric acid (1 mL, 0.005 N). A sector field inductive coupled plasma mass spectrometer (SF-ICP-MS), Thermo Electron Element II, housed at the High-Precision Spectrometry and Environment Change Laboratory (HISPEC), Department of Geosciences, National Taiwan University, was used to determine trace element/Ca ratios following the methodology developed by Shen et al. (2007). The detailed cleaning procedure and methodology are available in Lo et al. (2014). Two-year 1-sigma reproducibility of Mg/Ca analyses is ±0.21% (Lo et al., 2014). We used a composite Mg/Ca-SST equation by Anand et al. (2003) to calculate SSTs.

For oxygen stable isotope analysis, 7-10 individuals were immersed in methanol, ultrasonicated for 10 seconds, and then rinsed with deionized water 5 times. Samples were immersed afterward in a hyperchloride sodium (NaOCl) for 24 hours, and then analyzed with an isotopic ratio mass spectrometer (IRMS), Micromass IsoPrime, housed in the National Taiwan Normal University. Long-term 1-sigma precision is better than ±0.05‰ (N = 701, Lo et al., 2013) and data are reported with respect to Vienna Pee Dee Belemnite (VPDB).

To extract seawater $\delta^{18}O$ ($\delta^{18}O_{SW}$) values, we used a cultural based equation, $SST = 16.5 - 4.8 \times (\delta^{18}O_C - \delta^{18}O_{SW})$ (Bemis et al., 1998) and a constant offset of 0.27‰ between carbonate VPDB and Vienna Standard Ocean Water (VSMOW) scales. Ice volume corrected $\delta^{18}O_{SW}$ ($\delta^{18}O_{SW\text{-}IVC}$) was calculated using the method proposed by Waelbroeck et al. (2002).

The empirical orthogonal function (EOF) analysis of a modern SST dataset (1950-2004 AD, Reynolds et al., 2002) for a sector from 20°S – 20°N, and 100°E- 180°E was conducted (Fig. 2) to determine the boundary between N- and S-IPWP. With an equatorial border, the EOF1 factor (83.4%) clearly resolved different SST variation groups. The EOF2 factor shows minor (9.7%) but significant inter-annual zonal (ENSO) control on the SST patterns. EOF results show that the geographic equator is also the thermal equator between N-IPWP and S-IPWP (Fig. 2).

To build a stacked N- and S-IPWP record, we followed the suggestions by Leduc et al. (2010) and considered three criteria for this dataset: (1) sites with locations from 12°N to 15°S, which is the main IPWP range (Yan et al., 1992; Gagan et al., 2004), and (2) usage of specific proxies, Mg/Ca-derived SST and $\delta^{18}O_C$ records of planktonic foraminifera, *G. ruber* (white, *s.s.*). Records from 12 sites were selected, including this study (Table 2). We adopted the published age model for sites ODP806, MD97-2140, MD97-2141, MD98-2162, MD98-2170, MD98-2176, and MD98-2181. For records with available original radiocarbon ages from sites, including MD01-2378, MD01-2390, MD98-2165, and MD06-3067, we recalculated the age models using the CALIB 6.0.1 program. The sea level change effect on $\delta^{18}O_{SW}$ was also corrected. We divided the total data into 400-yr windows and calculated the mean and standard error of the mean for each time window.

3. Results and Discussion

3.1 Geochemical proxy data at site MD05-2925

Planktonic foraminiferal geochemical proxy data for site MD05-2925 are shown in Figure 3. *G. ruber* ä$^{18}O_C$ varies from -1.0 to -2.3‰ and shows no significant millennial timescale variations. Mg/Ca ratios feature stable glacial values of ~3.5 mmol/mol and rapid increasing transitions of 0.5-1.0 mmol/mol at ~18.5, 16.5, 14.5, and 12.8 ka. The glacial-interglacial variation of calculated seawater $\delta^{18}O_{SW}$ changes is ~1‰. Two abrupt decreases of 0.6-0.8‰ are observed at 14.6 and 11.8 ka.

3.2 Solomon SST and $\delta^{18}O_{SW\text{-}IVC}$ records during the last termination

Mg/Ca SST records of the planktonic foraminifera *G. ruber* reveal a stable glacial thermal condition during the period 23.0-18.5 ka, with a variation <1 ^{o}C and a glacial-interglacial difference of ~3 ^{o}C between the last glacial maximum (LGM) and the end of the Younger Dryas (YD) in the Solomon Sea (Fig. 4A). This record is characterized by (i) the end of glacial conditions at 18.5 ka, and (ii) rapid SST increases of 1-2 ^{o}C at 18.5-18.0, 17.0-16.0, 15.0-14.5, and 13.0-12.5 ka.

The onset of deglacial SST increases in this region is consistent with the timing of thermal changes in the Southern Ocean as inferred from Antarctic ice core δD records (Stenni et al., 2003) (Fig. 4A). This agreement indicates a strong climatic teleconnection between low- and high-latitude realms in the Southern Hemisphere (SH), as well as change of greenhouse gas concentrations (Mothadi et al., 2014). There are significant SST increases of 1-2 ^{o}C during Heinrich event (H1) and the YD. Previous studies from the Eastern Equatorial and South Pacific reveal a mechanism characterized by early warming of South Pacific subtropical mode water (Pahnke et al., 2003;

167 Lamy et al., 2004; Pena et al., 2008). This warm signal is transported along a
168 gyre to the east equatorial Pacific (EEP) and eventually to the west Pacific
169 through ocean tunneling (Pena et al., 2008; Qu et al., 2013, Fig. 4A). Our new
170 SST record is similar to those in the EEP (Pena et al., 2008) and eastern
171 Indian Ocean records (Xu et al., 2008; Mothadi et al., 2014) for both
172 termination timing (within dating error) and significant warming during the H1
173 and YD events. There is a slightly warming (<1 ^{o}C) interval at 14.5-13.5 ka
174 during the B/A period (Fig. 4A). The warming could be attributed to a possible
175 mixing with the warm N-IPWP surface water.

176 The Solomon Sea $\delta^{18}O_{SW\text{-}IVC}$ record is given in Figure 4B. It varies from -
177 0.5 to 0.1‰ during 23.0-10.5 ka. A relatively stable condition with 1-sigma
178 variability of 0.1‰ occurred from 23.0 to 16.0 ka. Two significant positive
179 excursions with 0.2-0.5‰ enrichments in $\delta^{18}O$ are observed in the intervals
180 16.8-15.0, and 13.8-11.8 ka. Two stable periods with low $\delta^{18}O_{SW\text{-}IVC}$ of -0.4‰
181 occurred between 15.0-13.0 ka and after 11.8 ka.

182 The dramatic $\delta^{18}O_{SW\text{-}IVC}$ increases during H1 and the YD likely resulted
183 from a weakening and/or southward shift of the ITCZ (Chiang and Bitz, 2005;
184 Broccoli et al., 2006), and local evaporation may also play a role. Agreement
185 of $\delta^{18}O$ sequences of Greenland NGRIP ice core and the Solomon Sea
186 $\delta^{18}O_{SW\text{-}IVC}$ indicates an imprint from high latitude Northern Hemisphere (NH)
187 during the last termination period (Shakun and Carlson, 2010) (Fig. 4B).

188

189 **3.3 Millennial timescale variations of N- and S-IPWP SST stacks**

190 Both N- and S-IPWP stacked SSTs show the same difference of ~3 ^{o}C
191 between the last glacial and interglacial states (Fig. 5A). N-IPWP stacked SST

values increased steadily since 18 ka through the termination at a rate of 0.5 ^{o}C/kyr. Millennial timescale variability is absent in this record, which is similar to Linsley et al. (2010) and Stott et al. (2002). Although the resolution of ODP 806 and MD97-2140 are less than our request to solve millennial-timescale event, there is no significant difference with/without their records in our N-IPWP stacks (not shown).

The onset of the termination at ~19 ka in the S-IPWP stack is consistent with temperature increases in Antarctica (Stenni et al., 2003), and occur about 1 kyr earlier than in the N-IPWP stack (Fig. 5A). This timing is synchronous with EEP (Pena et al., 2008) and non-upwelling region eastern Indian Ocean (Xu et al., 2008; Mothadi et al., 2014) SST records. Thus, our MD05-2925 and S-IPWP stacked SST may not severely controlled by the equatorial upwelling intensity. Instead of that, S-IPWP stacked SST represents broad SH equatorial region thermal conditions under upwelling/non-upwelling, E-W equatorial and even in the different ocean basins (Indian/Pacific Ocean). Records from the tropical South China Sea show inter-proxy ($U^{K'}_{37}$ and Mg/Ca) differences during the H1 and YD (Zhao et al.2006; Steinke et al., 2008), probably attributed to the intrinsic limitations of different proxies, such as seasonality and upwelling intensity. S-IPWP stacked SST record is characterized by a warming trend during H1 and the YD periods, similar to Antarctic ice core temperature records (Stenni et al., 2003), and a steady thermal condition at ~27 ^{o}C during Bølling/Allerød (B/A), corresponding to the Antarctic Cold Reversal (ACR) (Fig. 5A).

The thermal gradient between N- and S-IPWP is around 1 ^{o}C during 23 to 19 ka. Due to the earlier S-IPWP warming, the thermal gradient dropped from

1 to 0.5 ^{o}C around 19-18 ka, and persisted to the end of the H1 event. The largest observed thermal gradient (1.5-2.0 ^{o}C) occurred during the B/A period, and was followed by a 1 ^{o}C drop during the YD. The meridional SST gradient between N- and S-IPWP over the last termination is attributed to the large thermal variability in the S-IPWP (Fig. 5A). Asynchroneity between persistent N-IPWP and fluctuating S-IPWP SST sequences (Fig. 5A) indicates a meridionally dynamic IPWP through the last termination period. This N-S SST gradient variability would also affect interhemispheric air flow and heat transport (Gibbons et al., 2014; McGee et al., 2014), providing a mechanism to explain heat transport between the hemispheres on a millennial timescale.

3.4 N- and S-IPWP $\delta^{18}O_{SW\text{-}IVC}$ records

Both N- and S-IPWP $\delta^{18}O_{SW\text{-}IVC}$ records feature (i) low values of -0.3-0.0‰ during glacial times, and (ii) increasing trends after 19 ka (Fig. 5C). The gradient between N- and S-IPWP gradually increased from 0‰ to 0.2‰ through the termination (Fig. 5D). A similar pattern of $\delta^{18}O_{SW\text{-}IVC}$ between N- and S-IPWP suggests that hydrological conditions in the two regions were governed by the same factor(s), probably related to Northern Atlantic cold perturbations (Shakun and Carlson, 2010). It has also been suggested that a major $\delta^{18}O_{SW\text{-}IVC}$ increase during the H1 and YD periods in the IPWP region likely resulted from reduced precipitation and oceanic advection in both the N-IPWP and S-IPWP regions (Gibbsons et al., 2014; McGee et al., 2014).

3.5 Meridional IPWP SST gradient and the southward-shifted ITCZ precipitation boundary

A striking feature of the stacked SST records is the warming in the S-IPWP during the H1 and YD periods (Fig. 5A). Observations over the past six decades (Fig. 12 of Feng et al., 2013) show that an equatorward shift of the NH convection branch of the Hadley Cell (HC) could result from an oceanic warming at ~10^{o} S. This equatorward shift could induce a southward ITCZ shift of about 10^{o} (Feng et al., 2013). Model simulations (Chiang and Bitz, 2005; Broccoli et al., 2006, Lee et al., 2011) suggest that this altered circulation is a powerful teleconnection between the NH and SH climate systems through a coupled tropical ocean-atmosphere pathway, and is supported by marine and terrestrial hydrological proxy data (Wang et al., 2001, Lea et al., 2003, Wang et al., 2007,Griffiths et al., 2009, Shakun and Carlson, 2010, Mohtadi et al., 2011, Meckler et al., 2012, Ayliffe et al., 2013, Carolin et al., 2013, Gibbons et al., 2014; McGee et al., 2014, Fig. 6).

Distinctly different precipitation conditions across 8-10^{o}S in the IPWP during the H1 and YD events are illustrated in Figure 6. For example, enhanced terrestrial sediment flux into the Coral Sea is suggested by a marine sediment thorium isotopic proxy record at 11^{o} S (Shiau et al. 2011). Lynch's crater records from northeastern Australia at 17^{o} S (Muller et al., 2008) show strong Australian summer monsoonal conditions. Stalagmite $\delta^{18}O$ records at Flores Island (8^{o} S) also feature intense precipitation during H1 and the YD (Griffiths et al., 2009, Ayliffe et al., 2013). However, marine and stalagmite $\delta^{18}O$ evidence reveal conditions of reduced precipitation and increased salinity in the northern IPWP north of 8-10^{o} S, including the South China Sea (12^{o} N, Stenike et al., 2006), Sulu Sea (8^{o} N, Rosenthal et al., 2003), Philippine Sea (6^{o} N, Stott et al., 2002; Boillet et al., 2011), Java Island

267 (8° S, Mohtadi et al., 2011), Solomon Sea (9° S, this study), and Borneo island
268 (4° N, Meckler et al., 2012, Carolin et al., 2013) (Fig. 6). On the basis of
269 previous terrestrial and marine hydrological records and our new data, as well
270 as modern (Feng et al., 2013) and simulated (Chiang and Bitz, 2005: Broccoli
271 et al., 2006) data, we speculate a sharp precipitation boundary between the
272 maritime continents and Australia at about 8-10° S, extending from the
273 Solomon Sea, Arafura Sea and Timor Sea, to the eastern Indian Ocean
274 during H1 and the YD periods (Fig. 6). We propose that the west and east
275 boundaries are between the Java-Flores islands (Griffiths et al., 2009,
276 Mohtadi et al., 2011), and Solomon-Coral Seas, respectively (Shiau et al.,
277 2011, this study). Geographical mismatch between N- and S-IPWP thermal
278 and precipitation patterns could be associated with the complex of island
279 mountain range configurations and sea level change (Linsley et al., 2010).
280 To sum up our geochemical and composite dataset in the IPWP region
281 during the last terminations, we propose that the enlarged IPWP meridional
282 SST gradient could result in an altered HC and reduced (increased)
283 precipitation for the East Asian (Australia) monsoon territories during the H1
284 and YD periods (McGee et al., 2014). We also propose that variations in the
285 meridional IPWP SST gradient during the termination period were mainly
286 caused by the S-IPWP, which is closely linked to high-latitude climate
287 systems.
288

289 **4. Conclusions**

290 Our new MD05-2925 marine geochemical records and previous reports
291 suggest that the meridional IPWP thermal conditions are strongly linked to

interhemispheric high-latitude climate during the last deglaciation. Ice volume-corrected $\delta^{18}O_{SW}$ stacked records show an increasing salinity gradient between N- and S-IPWP over the last termination. Here we propose a new process of the thermal evolution of IPWP region, which meridional differences of its thermal gradient could amplify the signal from high latitude Northern hemisphere climate events, including H1, B/A and YD, and radiative forcing from greenhouse gases. A hypothetical precipitation boundary around 8-10^{o} S during H1 and the YD has also been proposed, which is most likely caused by the meridional IPWP SST gradient and HC anomalies. We suggest that more advanced high-resolution regional model simulations are required to clarify (1) local precipitation variations in response to the complicated sea level and convection changes, (2) the role of IPWP meridional thermal-hydrological gradient to an altered HC, and (3) its relationship with regional and global climate systems during global climate perturbation events.

Acknowledgements

MD05-2925 site location was selected by Min-Te Chen and Meng-Yang Lee and collected during the IMAGES PECTEN Cruise, conducted by Luc Beaufort and Min-Te Chen. Chien-Ju Chou, Wan-Lin Hu, and Yu-Ting Hsiao helped to pick foraminifera samples. Yang-Hui Hsu helped to operate the climatological database and plotted figures. Thanks to Delia W. Oppo and Braddock K. Linsley for their generous offering of the non-overlapping method MatLab code. This research was funded by Taiwan ROC MOST (99-2611-M-002-005, 100-2116-M-002-009 and 103-2119-M-002-022 to CCS; 95-2611-M-002-019 and 96-2611-M-002-019 to KYW), and National Taiwan University (101R7625 to CCS).

References

Anand, P. A., Elderfield, H., and Conte, M. H.: Calibration of Mg/Ca thermometry in planktonic foraminifera from a sediment trap time series. Paleoceanography, 18, 1050, doi:10.1029/2002PA000846, 2003.

Ayliffe, L. K., Gagan, M. K., Zhao, J.-x., Drysdale, R. N., Hellstrom, J. C., Hantoro, W. S., Griffiths, M. L., Scott-Gagan, H., Pierre, E. S, Cowley, J. A., and Suwargadi, B. W.: Rapid interhemispheric climate links *via* the Australasian monsoon during the last deglacialtion. Nature Commun., 4, doi: 10.1038/ncomms3908.

Bolliet, T., Holbourn, A., Kuhnt, W., Laj, C., Kissel, c., Beaufort, L., Kienast, M., Andersen, N., and Garbe-Schönberg, D.: Mindanao Dome variability over the last 160 kyr: Episodic glacial cooling of the West Pacific Warm Pool. Paleoceanography, 26, PA1208, doi: 10.1029/2010PA001966, 2011.

Broccoli, A. J., Dahl, K. A., and Stouffer, R. J.: Response of the ITCZ to Northern Hemisphere cooling. Geophys. Res. Lett., 33, L01702, doi: 10.1029/2005GL024546, 2006.

Carolin, S. A., Cobb, K. M., Adkins, J. F., Clark, B., Conroy, J. L., Lejau, S., Malang, J., and Tuen, A. A.: Varied response of Western Pacific hydrology to climate forcings over the last glacial period. Science, 340, 1564-1566, 2013.

Chiang, J. C. H., and Bitz, C. M.: Influence of high latitude ice cover on the marine Intertropical Convergence Zone. Clim. Dynam., 25, 477–496, 2005.

Cravatte, S., Delcroix, T., Zhang, D., McPhaden, M., and Leloup, J.: Observed freshening and warming of the western Pacific Warm Pool. Clim. Dynam., 33, 565–589, 2009.

de Garidel-Thoron, T., Rosenthal, Y., Bassinot, F., and Beaufort, L.: Stable sea surface temperatures in the western Pacific warm pool over the past 1.75 million years. Nature, 433, 294–298, 2005.

Feng, J., Li, J., and Xie, F.: Long-term variation of the Principal mode of boreal spring Hadley Circulation linked to SST over the Indo-Pacific Warm Pool. J. Clim., 26, 532-544, 2013.

Gibbons, F. T., Oppo, D. W., Mohtadi, M., Rosenthal, Y., Cheng, J., Liu, Z., and Linsley, B. K.: Deglacial $\delta^{18}O$ and hydrological variability in the tropical and Indian Oceans. Earth Planet. Sci. Lett., 387, 240-251, 2014.

Grenier, M., Cravatte, S., Blanke, B., Menkes, C., Joch-Larrouy, A., Durand, F., Melet, A., and Jeandel, C.: From the western boundary currents to the Pacific Equatorial Undercurrent: Modeled pathways and water mass evolutions. J. Geophys. Res., 116, C12044, doi: 10.1029/JC007477, 2011.

369 Griffiths, M. L., Drysdale, R. N., Gagan, M. K., Zhao, J.-X., Ayliffe, L. K.,
370 Hellstrom, J. C., Hantoro, W. S., Frisia, S., Feng, Y.-X., Cartwright, I., St.
371 Pierre, E., Fischer, M., J., and Suwargadi, B. W.: Increasing Australian-
372 Indonesian monsoon rainfall linked to early Holocene sea-level rise. Nature
373 Geosci., 2, 636–639, 2009.
374
375 Lamy, F., Kaiser, J., Ninnemann, U., Hebbeln, D., Arz, H. W., and Stoner, J.:
376 Antarctic timing of surface water changes off Chile and Patagonian ice
377 sheet response. Science, 304, 1959-1962, 2004.
378
379 Lea, D. W., Pak, D. K., and Spero, H. J.: Climate impact of late Quaternary
380 equatorial Pacific sea surface temperature variations. Science, 289, 1719-
381 1724, 2000.
382
383 Lea, D. W., Pak, D. K., Peterson, L. C., and Hughen, K. A.: Synchroneity of
384 tropical high-latitude Atlantic temperatures over the last glacial termination.
385 Science, 301, 1361-1364, 2003.
386
387 Leduc, G., Schneider, R., Kim, J.H., and Lohmann, G.: Holocene and Eemian
388 sea surface temperature trends as revealed by alkenone and Mg/Ca
389 paleothermometry. Quaternary Sci. Rev., 29, 989 – 1004, 2010.
390
391 Levi, C., Labeyrie, L., Bassinot, F., Guichard, F., Cortijo, E., Waelbroeck, C.,
392 Caillon, N., Duprat, J., de Garidel-Thoron, T., and Elderfield, H.: Low-
393 latitude hydrological cycle and rapid climate changes during the last
394 deglaciation. Geochem., Geophy., Geosy., 8(5), Q05N12, doi:
395 10.1029/2006GC001514, 2007.
396
397 Linsley, B. K., Rosenthal, Y., and Oppo, D. W.: Holocene evolution of the
398 Indonesian throughflow and the western Pacific warm Pool. Nature Geosci.,
399 3, 578–583, 2010.
400
401 Lo, L., Lai, Y.-H., Wei, K.-Y., Lin, Y.-S., Mii, H.-S., and Shen, C.-C.: Persistent
402 sea surface temperature and declined sea surface salinity in the
403 northwestern tropical Pacific over the past 7500 years. J. Asian Earth Sci.,
404 66, 234-239, 2013.
405
406 Lo, L., Shen, C.-C., Lu, C.-J., Chen, Y.-C., Chang, C.-C., Wei, K.-Y., Qu, D.,
407 and Gagan, M. K.: Determination of element/Ca ratios in foraminifera and
408 corals using cold- and hot-plasma techniques in inductively coupled plasma
409 sector field mass spectrometry. J. Asian Earth Sci., 81, 115-122, 2014.
410
411 McGee, D., Donohoe, A., Marshall, J., and Ferreira, D.: Changes in ITCZ
412 location and cross-equatorial heat transport at the Last Glacial Maximum,
413 Heinrich Stadial 1, and the mid-Holocene. Earth Planet. Sci. Lett., 390, 69-
414 79, 2014.
415
416 Meckler, A. N., Clarkson, M. O., Cobb, K. M., Sodemann, H., and Adkins, J. F.:
417 Interglacial hydroclimate in the tropical West Pacific through the late
418 Pleistocene. Science, 336, 1301-1304, 2012.

Melet, A., Verron, J., Gourdeau, L., and Koch-Larrouy, A.: Equatorial pathways of Solomon Sea water masses and their modification. J. Phys. Oceano., 40, 810–826, 2011.

Mohtadi, M., Oppo, D. W., Steinke, S., Stuut, J.-B. W., De Pol-Holz, R., Hebbeln, D., and Lückge, A.: Glacial to Holocene swings of the Australian-Indonesian monsoon. Nature Geosci., 4, 540–544, 2011.

Mothadi, M. Prange, M., Oppo, D. W., De Pol-Holz, R., Merkel, U., Zhang, X., Stenike, S., and Lückge, A.: North Atlantic forcing of tropical Indian Ocean climate. Nature 509, 76-80, 2014.

Muller, J., Kylander, M., Wüst, R. A. J., Weiss, D., Martinez-Cortizas, A., LeGrande, A. N., Jennerjahn, T., Behling, H., Andreson, W. T., and Jacobson, G.: Possible evidence for wet Heinrich phases in tropical Australia: the Lynch's Crater deposit. Quaternary Sci. Rev., 27, 468–475, 2008.

Northern Greenland Ice Core Project Members: High-resolution record of Northern Hemisphere climate extending into the last interglacial period. Nature, 431, 147–151, 2004.

Oppo, D. W., Rosenthal, Y., and Linsley, B. K.: 2,000-year-long temperature and hydrology reconstructions from the Indo-Pacific warm pool. Nature, 460, 1113–1116, 2009.

Pahnke, K., Zahn, R., Elderfield, H., and Schulz, M.: 340,000-year centennial-scale marine record of Southern Hemisphere climatic oscillation. Science, 301, 948-952, 2003.

Pena, L. D., Cacho, I., Ferretti, P., and Hall, M. A.: El Niño-Southern Oscillation-like variability during glacial terminations and interlatitudinal teleconnections. Paleoceanography, 23, PA3101, doi: 10.1029/2008PA001620, 2008.

Qu, T., Gao, S., and Fine, R. A.: Subduction of South Pacific tropical water and its equatorward pathways as shown by a simulated passive tracer. J. Phys. Oceanogr., 43, 1551-1565, 2013.

Reimer, P. J., Baillie, M. G. L., Bard, E., Bayliss, A., Beck, J. W., Blackwell, P. G., Bronk Ramsey, C., Buck, C. E., Burr, G. S., Edwards, R. L., Friedrich, M., Grootes, P. M., Guilderson, T. P., Hajdas, I., Heaton, T. J., Hogg, A. G., Hughen, K. A., Kaiser, K. F., Kromer, B., McCormac, F. G., Manning, S. W., Reimer, R. W., Richards, D. A., Southon, J. R., Talamo, S., Turney, C. S. M., van der Plicht, J., and Weyhenmeyer, C. E.: INTCAL09 and MARINE09 radiocarbon age calibration curves, 0-50,000 cal BP. Radiocarbon 51(4): 1111-1150, 2009.

Reynolds, R. W., Rayner, N. A., Smith, T. M., and Stokes, D. C.: An improved in situ and satellite SST analysis for climate. J. Clim., 15, 1609–1625, 2002.

Rosenthal, Y., Oppo, D. W., and Linsley, B. K.: The amplitude and phasing of climate change during the last deglaciation in the Sulu Sea, western equatorial Pacific. Geophys. Res. Lett., 30(8), 1428, doi: 10.1029/2002GL016612, 2003.

Shakun, J. D., and Carlson, A. E.: A global perspective on Last Glacial maximum to Holocene climate change. Quaternary Sci. Rev., 29, 1801-1816, 2010.

Shakun, J. D., Clark, P. U., He, F., Marcott, S. A., Mix, A. C., Liu, Z., Otto-Bliesner, B., Schmittner, A., and Bard, E.: Global warming preceded by increasing carbon dioxide concentrations during the last deglaciation. Nature, 484, 49-55, 2012

Shen, C.-C., Hasting, D. W., Lee, T., Chiu, C.-H., Lee, M.-Y., Wei, K.-Y., and Edwards, R. L.: High precision glacial-interglacial benthic foraminiferal Sr/Ca records from the eastern equatorial Atlantic Ocean and Caribbean Sea. Earth Planet. Sci. Lett., 190, 197-209, 2001.

Shen, C.-C., Chiu, H.-Y., Chiang, H.-W., Chu, M.-F., Wei, K.-Y., Steinke, S., Chen, M.-T., Lin, Y.-S., and Lo, L.: High precision measurements of Mg/Ca and Sr/Ca ratios in carbonates by cold plasma inductively coupled plasma quadrupole mass spectrometry. Chem. Geol., 236, 339-249, 2007.

Shiau, L.-J., Chen, M.-T., Clemens, S. C., Huh, C.-A., Yamamoto, M., and Yokoyama, Y.: Warm pool hydrological and terrestrial variability near southern Papua New Guinea over the past 50k. Geophys. Res. Lett., 38, L00F01, doi: 10.1029/2010GL045309, 2011.

Shiau, L.-J., Chen, M.-T., Huh, C.-A., Yamamoto, M., and Yokoyama, Y.: Insolation and cross-hemispheric controls on Australian monsoon variability over the past 180 ka: New evidence from off shore southeastern Papua New Guinea. J. Quaternary Sci., 27, 911-920, 2012.

Steinke, S., Chiu, H.-I., Yu, P.-S., Shen, C.-C., Erlenkeuser, H., Löwemark, L., and Chen, M.-T.: On the influence of sea level and monsoon climate on the southern South China Sea freshwater budget over the past 22,000 years. Quaternary Sci. Rev., 25, 1475–1488, 2006.

Stenike, s., Kienast, M., Groeneveld, J., Lin, L.-C., Chen, M.-T., and Rendle-Bühring, R.: Proxy dependence of the temporal pattern of deglacial warming in the tropical South China Sea: toward resolving seasonality. Quaternary Sci. Rev., 27, 688-700, 2008.

Stenni, B., Jouzel, J., Masson-Delmotte, V., Röthlisberger, R., Castellano, E., Cattani, O., Falourd, S., Johnsen, S. J., Longinelli, A., Sachs, J. P., Selmo, E., Souchez, R., Steffensen, J. P., and Udisti, R.: A late-glacial high-

518 resolution site and source temperature record derived from EPICA Dome C
519 isotope records (East Antarctica). Earth Planet. Sci. Lett., 217, 183–195,
520 2003.
521
522 Stott, L., Cannariato, K., Thunell, R., Haug, G. H., Koutavas, A., and Lund, S.:
523 Decline of surface temperature and salinity in the western tropical Pacific
524 Ocean in the Holocene epoch. Nature, 431, 56–59, 2004.
525
526 Stott, L., Poulsen, C., Lund, S., and Thunell, R.: Super ENSO and global
527 climate oscillations at millennial time scales. Science, 297, 222-226, 2002.
528
529 Stuiver, M., Reimer, P. J., and Reimer, R. W.: CALIB 6.0. (WWW program
530 and documentation), 2010.
531
532 Visser, K., Thunell, R., and Stott, L.: Magnitude and timing of temperature
533 change in the Indo-Pacific warm pool during deglaciation. Nature, 421,
534 152–155, 2003.
535
536 Wang, Y. J., Cheng, H., Edwards, R. L., An, Z. S., Wu, J. Y., Shen, C.-C., and
537 Dorale, J. A.: A high-resolution absolute-dated late Pleistocene monsoon
538 record from Hulu Cave, China. Science, 294, 2345-2348, 2001.
539
540 Wang, X., Auler, A. S., Edwards, R. L., Cheng, H., Ito, E., Wang, Y., Kong, X.,
541 and Solheid, M.: Millennial-scale precipitation changes in southern Brazil
542 over the past 90,000 years. Geophys. Res. Lett., 34, L23701,
543 doi:10.1029/2007GL031149, 2007.
544
545 Williams, A. P, and Funk, C.: A westward extension of the warm pool leads to
546 a westward extension of the Walker circulation, drying eastern Africa. Clim.
547 Dynam., 37, 2417–2435, 2011.
548
549 Xu, J., Holbourn, A., Kuhnt, W., Jian, Z., and Kawamura, H.: Changes in ther
550 thermocline structure of the Indonesian outflow during Terminations Ⅰ and
551 Ⅱ. Earth Planet. Sci. Lett., 273, 152–162, 2008.
552
553 Yan, X.-H., Ho, C.-R., Zheng, Q., and Klemas, V.: Temperature and size
554 variabilities of the western Pacific warm pool. Science, 258, 1643-1645,
555 1992.
556
557 Zhao, M., Huang, C.-Y., Wang, C.-C., and Wei, G.: A millennial-scale $U^{K'}_{37}$
558 sea surface temperature record from the South China Sea (8 ^{o}N) over the
559 last 150 kyr: Monsoon and sea-level influence. Palaeogeogr.
560 Palaeoclimatol Palaeoecol, 236, 39-55, 2006.
561

562 **Table 1** AMS ^{14}C dates of site MD05-2925.

Depth (cm)	^{14}C ages (years)	Error (years)	Cal. ages (years)	Error (years)
117	8823	50	9414	111
127*	10306	70	11259	159
140	10441	30	11333	80
147*	11477	70	12854	110
157	12066	60	13391	84
172*	13117	70	14973	309
180	13748	35	16283	453
192*	14080	74	16746	223
207*	15616	75	18201	175
217	16470	81	19083	90
262*	18985	94	22167	181
272*	20960	150	24411	167
292*	21650	78	25304	339

563

564 *Samples were measured in the NSF-Arizona AMS Laboratory of the
565 University of Arizona (U. Arizona), Tucson, USA, and the others were
566 measured in the Rafter Radiocarbon Laboratory, Institute of Geological and
567 Nuclear Science (GNS), New Zealand.
568
569

570

571

572

573

574

575 **Table 2** Selected sites for stacked N- and S-IPWP records.

Core	Location (Latitude, and longitude)	References
North-IPWP group (orange circles in Figs 1 and 2)		
ODP 806	0.3°N, 159.4°E	Lea et al. (2000)
MD97-2140	2.0°N, 141.7°E	de Garidel-Thoron et al. (2005)
MD98-2181	6.3°N, 125.8°E	Stott et al. (2002, 2004)
MD06-3067	6.5°N, 126.5°E	Bolliet et al. (2011)
MD97-2141	8.8°N, 121.3°E	Rosenthal et al. (2003)
MD01-2390	12.1°N, 113.2°E	Stenike et al. (2006)
South-IPWP group (green circles and star in Figs 1 and 2)		
MD98-2162	4.4°S, 117.5°E	Visser et al. (2003)
MD98-2176	5.0°S, 133.4°E	Stott et al. (2004)
MD05-2925	9.3°S, 151.5°E	This Study
MD98-2165	9.7°S, 118.3°E	Levi et al. (2007)
MD98-2170	10.6°S, 125.4°E	Stott et al. (2004)
MD01-2378	13.1°S, 121.7°E	Xu et al. (2008)

576
577

Figure captions

Fig. 1. Climatological map of the Indo-Pacific Warm Pool (IPWP) sea surface temperature (SST, left) and precipitation (right) during 1950-2004 AD (Reynolds et al., 2002). Upper panels are June-July-August (JJA), and lower panels are December-January-February (DJF) averages of **(A, C)** SSTs and **(B, D)** precipitation distribution maps. SST and precipitation are at 0.5 ^{o}C and 2 mm/day intervals. Our study site MD05-2925 is shown as the green star. Orange and green dots denote previous study sites in the IPWP region (Table 2) for reconstruction of meridional thermal and precipitation variations during the glacial/interglacial change.

Fig. 2. EOF analysis on SST (Dataset from Reynolds et al., 2002) and selected sites (Table 2) used for stacked N- and S-IPWP records. **(A)** EOF1 explains 83.4% of the total variance, which mainly represents intra-annual seasonality. **(B)** EOF2 shows a clear zonal pattern. Orange circles represent selected sites for the N-IPWP group and green ones for the S-IPWP group. The green star denotes the MD05-2925 site used in this study.

Fig. 3. Planktonic foraminifera *G. ruber* geochemical proxy records of site MD05-2925, including **(A)** oxygen isotope ($\delta^{18}O_C$), **(B)** Mg/Ca ratio, and **(C)** temperature corrected-only seawater oxygen isotope ($\delta^{18}O_{SW}$). Triangle symbols are corrected radiocarbon dates (Table 1).

Fig. 4. Geochemical proxy records of MD05-2925. **(A)** SST (red circles and line) and **(B)** $\delta^{18}O_{SW\text{-}IVC}$ (blue line) were reconstructed with *G. ruber* Mg/Ca ratios and $\delta^{18}O_C$. The cyan line denotes the Antarctica EPICA deuterium isotope record (Stenni et al., 2003), and the yellow line is the Greenland ice core NGRIP (Northern Greenland Ice Core Project Members, 2004) oxygen isotope record. The superimposed dark cyan and dark yellow lines are the 200-yr smoothed records, respectively. Black triangles are AMS ^{14}C dates (Table 1). Vertical bars denote the H1 and YD periods.

Fig. 5. Four hundred-year non-overlapping binned **(A)** SST and **(C)** $\delta^{18}O_{SW\text{-}IVC}$ of N- (orange solid line) and S-IPWP (green solid line). Lower panel show the differences in **(B)** SST and **(D)** $\delta^{18}O_{SW\text{-}IVC}$ between N- and S-IPWP. The compilations of N- and S-IPWP surface water thermal and hydrological records (Table 2) were calculated with the non-overlapping binned methods (Oppo et al., 2009; Linsley et al., 2010). All dashed lines represent 1-sigma uncertainty ranges. Gray bars show the H1 and YD events.

Fig. 6. Hypothetical proxy-inferred precipitation boundary during the H1 and YD events (modified from the Linsley et al., 2010). Blue dots represent relatively increasing precipitation/$\delta^{18}O_{SW}$ lighter condition, and brown ones a decreasing precipitation/ä$^{18}O_{SW}$ heavier condition. The segment between Java and Flores Islands of this sharp boundary (red dashed line) was proposed by Mohtadi et al. (2011), and the one between the Solomon and Coral Seas by this study. Black contours represent SST.

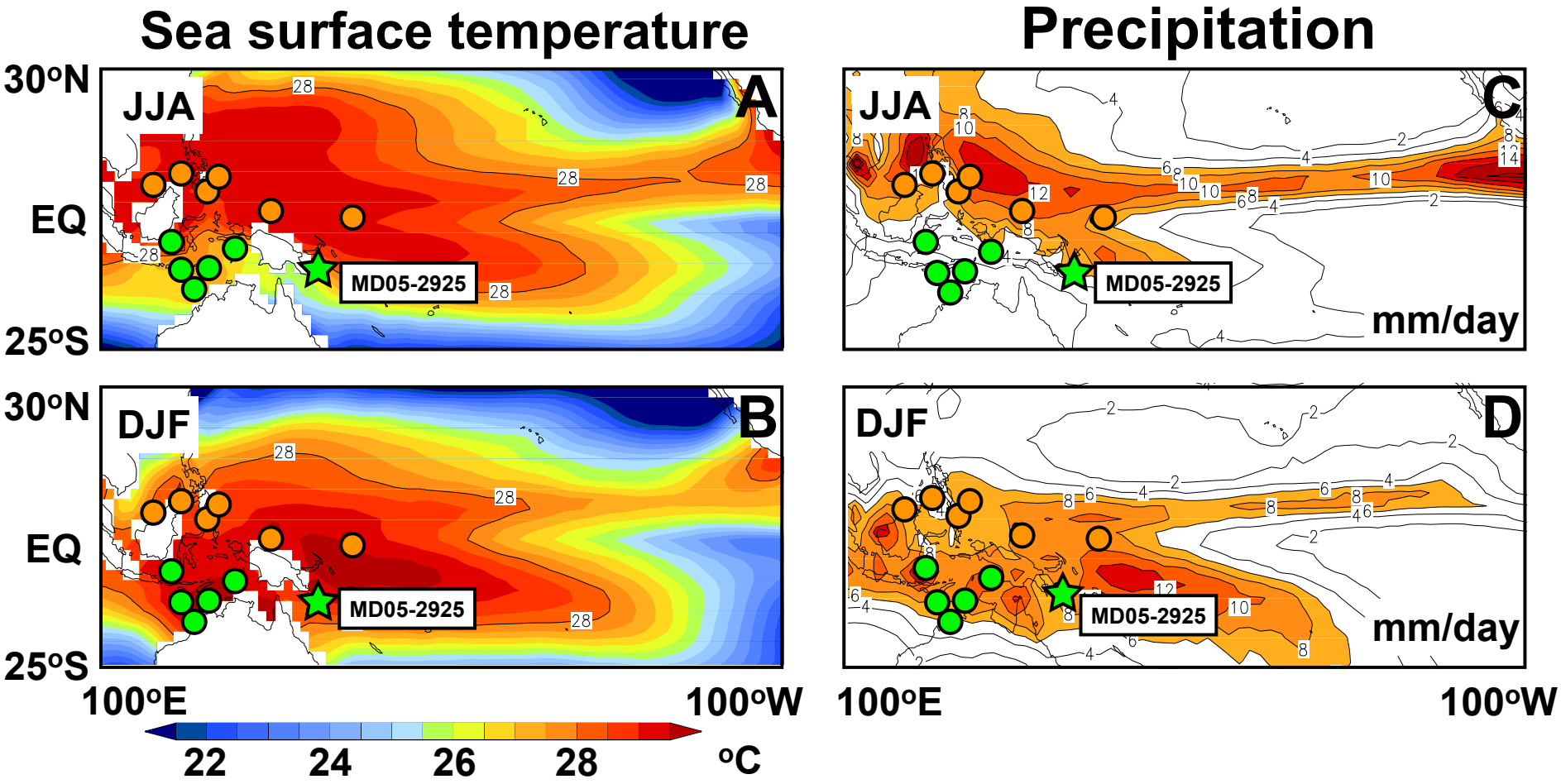
Sea surface temperature
Precipitation
30°N
EQ
25°S
JJA
DJF
A
B
C
D
MD05-2925
mm/day
100°E
100°W
22
24
26
28
°C

Fig. 1

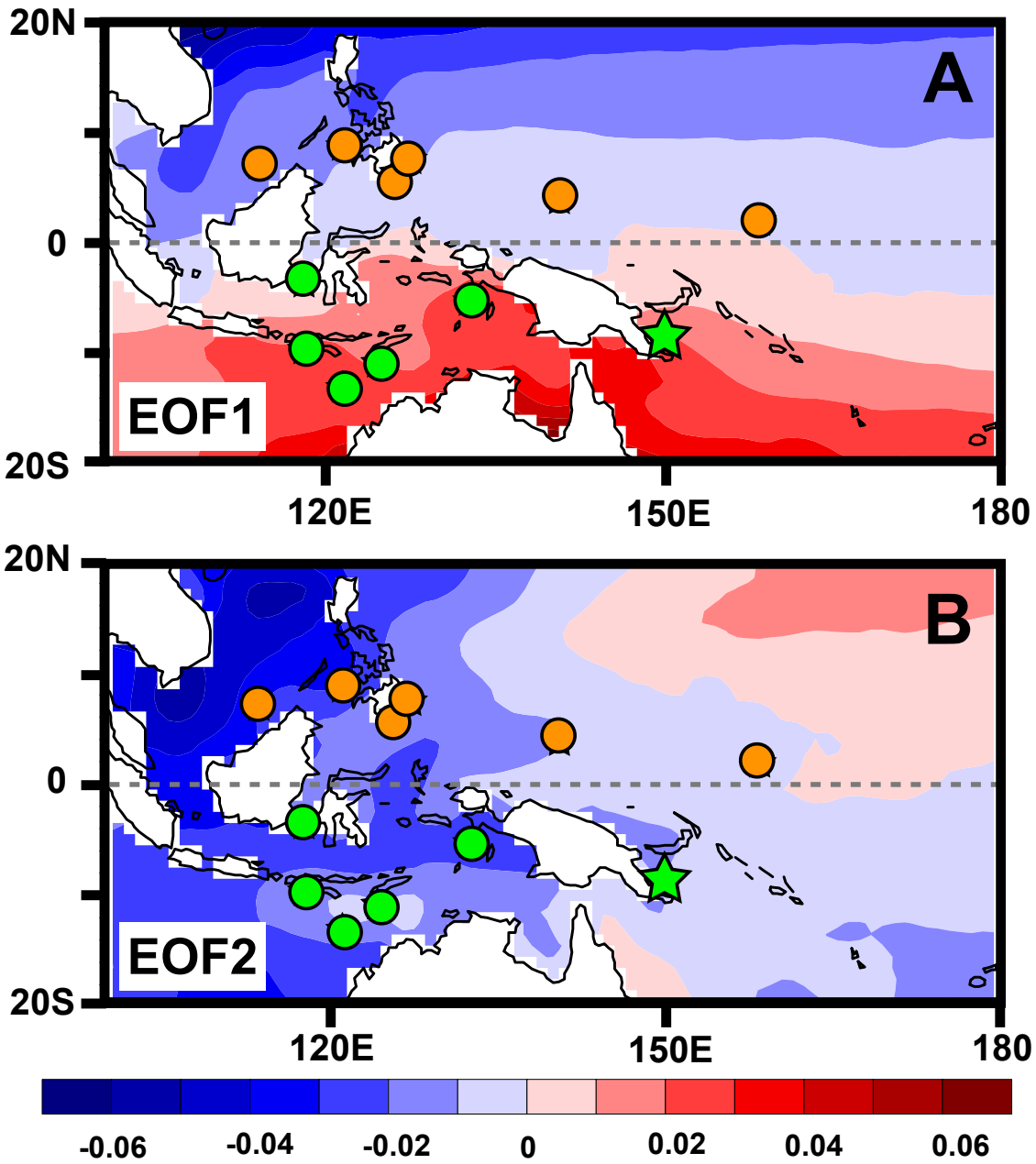

Fig. 2

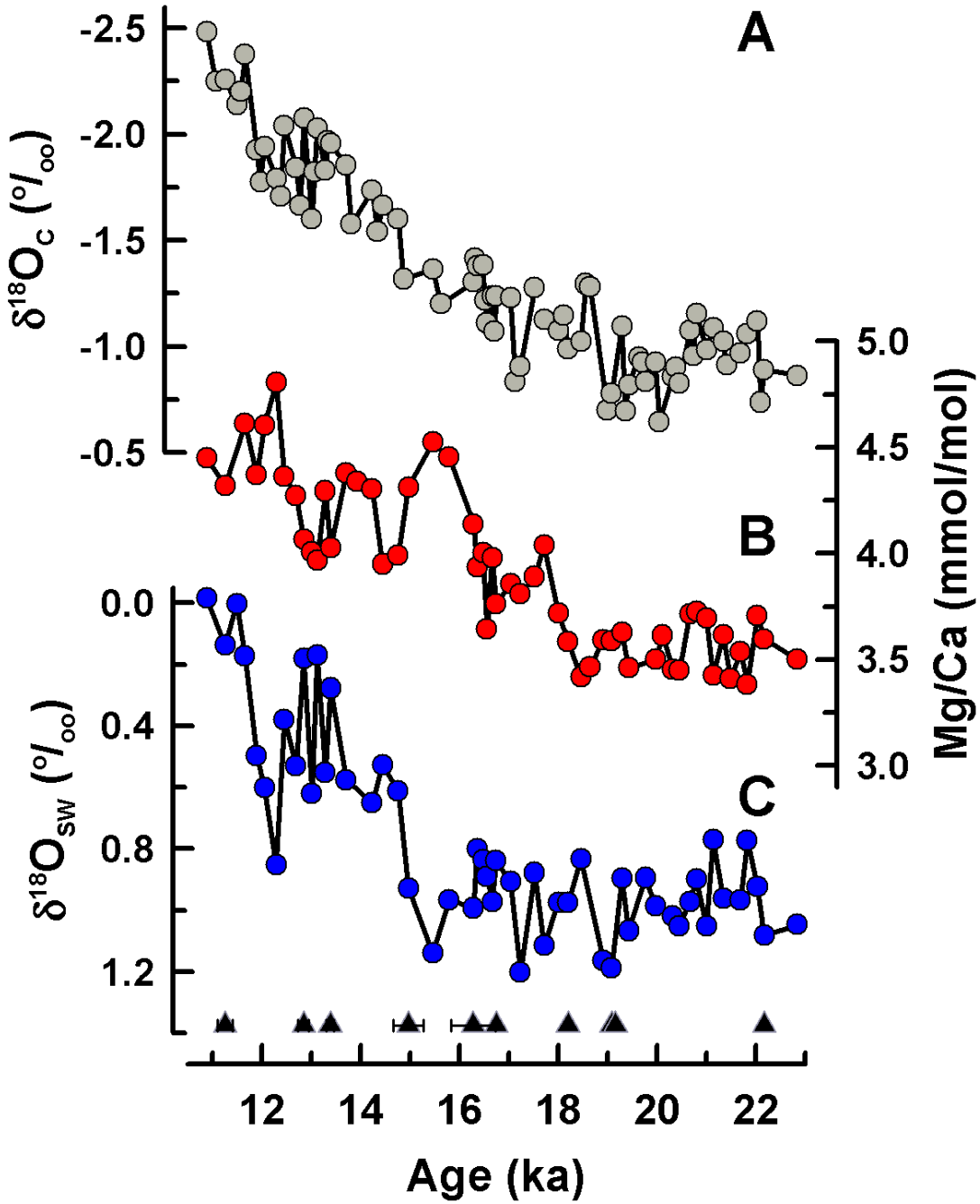
A
B
C
-2.5
-2.0
-1.5
-1.0
-0.5
δ18OC (°/oo)
5.0
4.5
4.0
3.5
3.0
Mg/Ca (mmol/mol)
0.0
0.4
0.8
1.2
δ18OSW (°/oo)
12
14
16
18
20
22
Age (ka)

Fig. 3

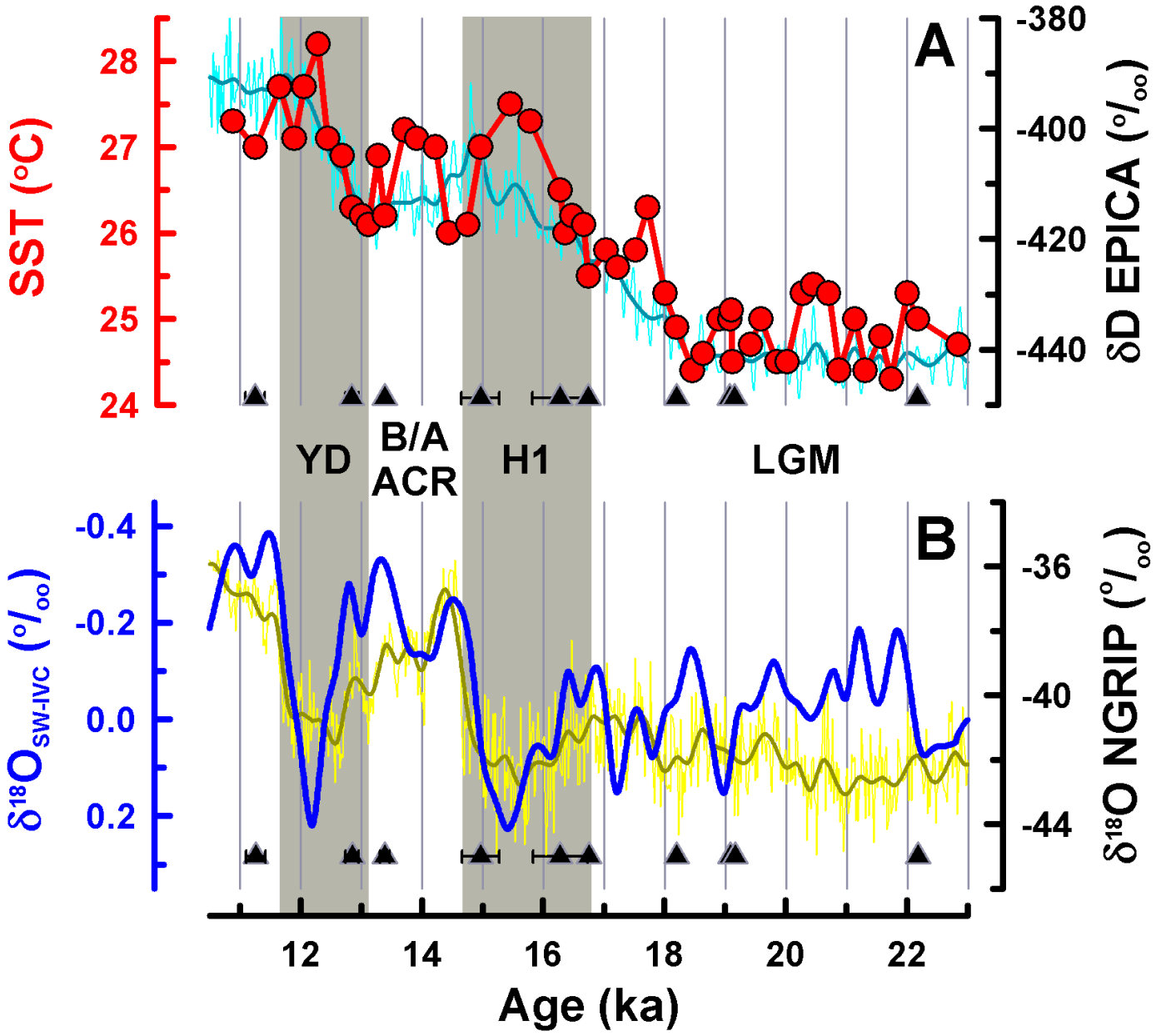
A
B
SST (°C)
28
27
26
25
24
δD EPICA (°/oo)
-380
-400
-420
-440
YD
B/A
ACR
H1
LGM
δ18OSW-IVC (°/oo)
-0.4
-0.2
0.0
0.2
δ18O NGRIP (°/oo)
-36
-40
-44
12
14
16
18
20
22
Age (ka)

Fig. 4

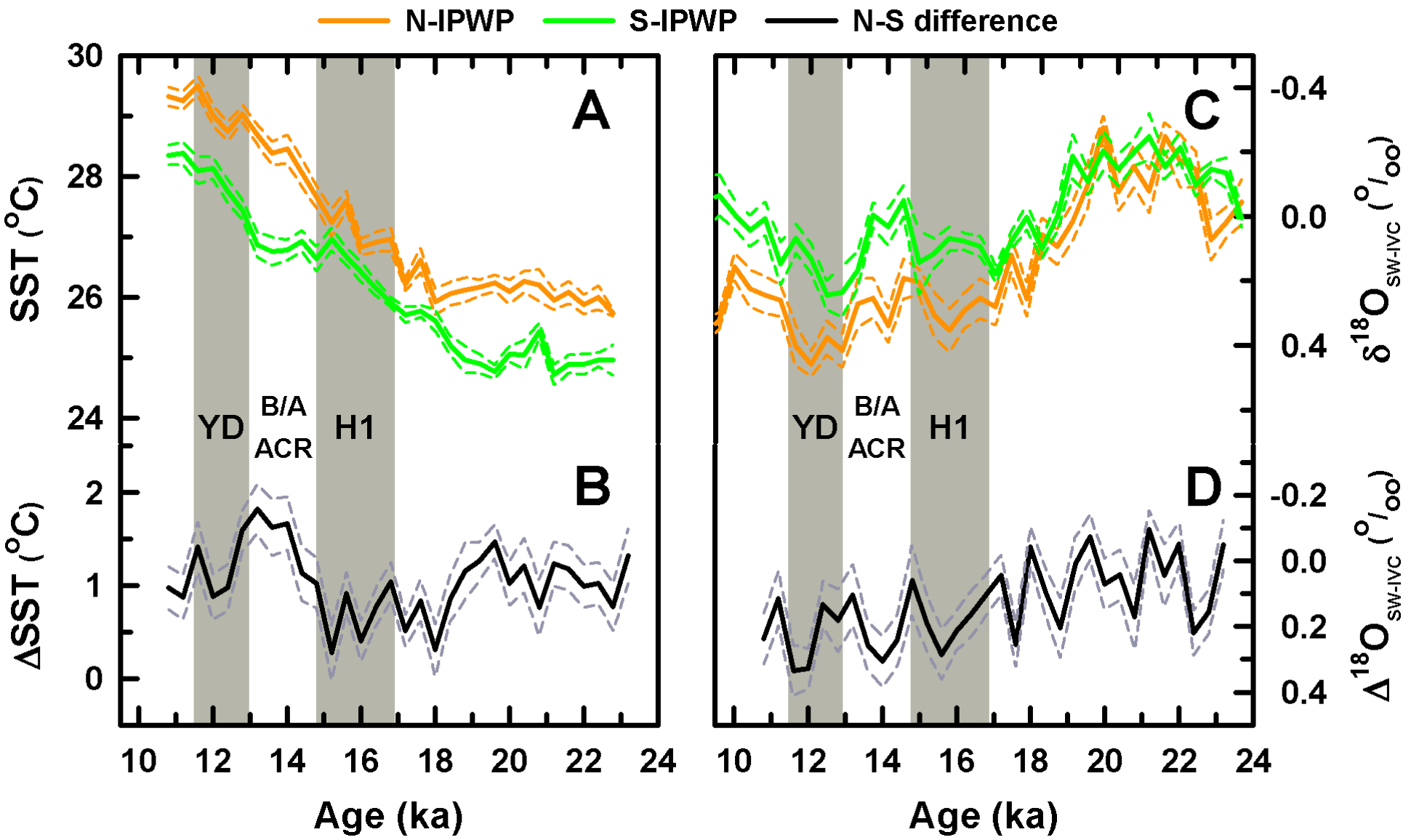
N-IPWP
S-IPWP
N-S difference
A
B
C
D
YD
B/A
ACR
H1
SST (°C)
ΔSST (°C)
δ18OSW-IVC (°/oo)
Δ18OSW-IVC (°/oo)
Age (ka)
Age (ka)

Fig. 5

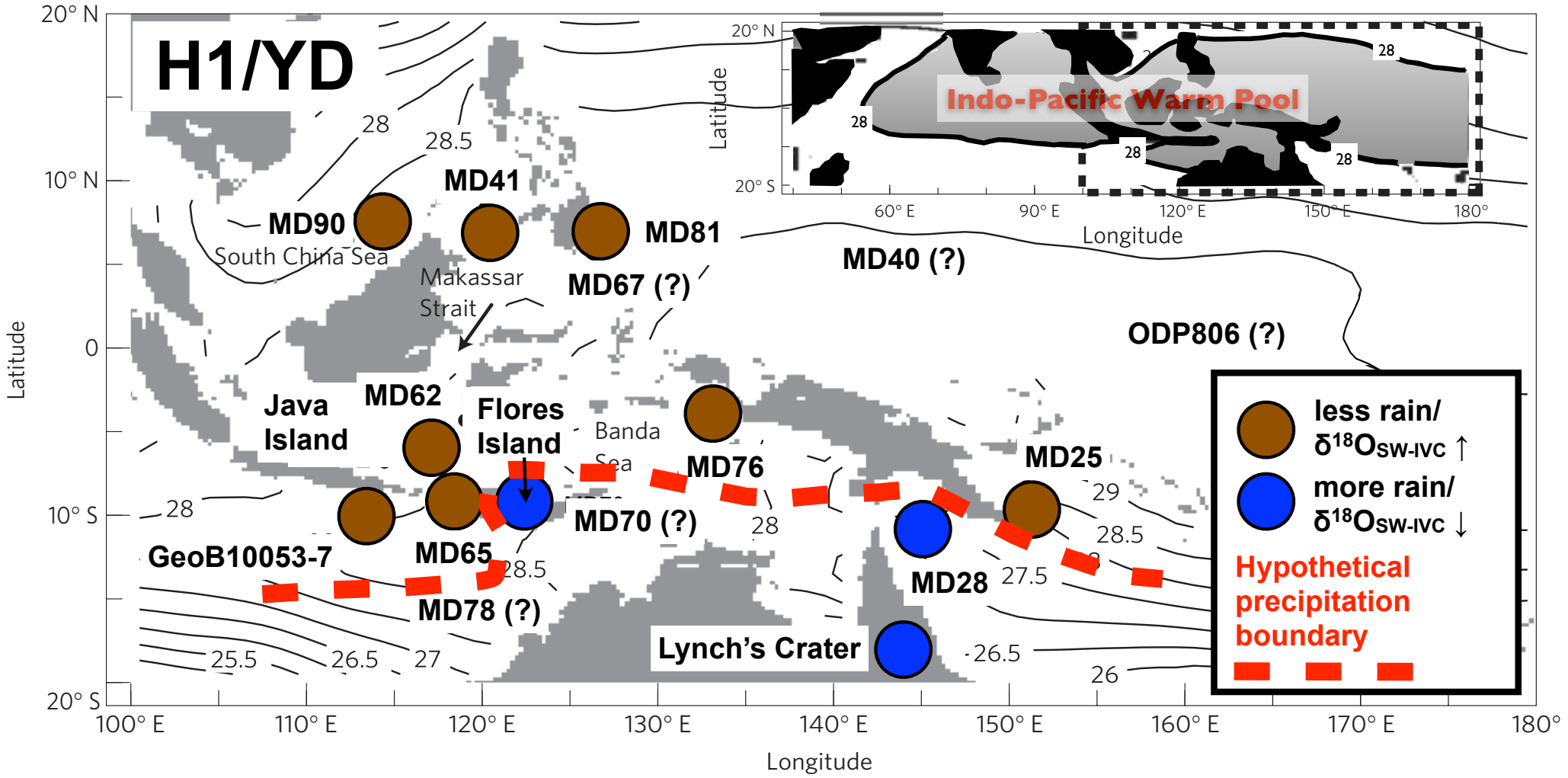
H1/YD
MD90
South China Sea
MD41
MD81
MD67 (?)
Makassar Strait
MD40 (?)
ODP806 (?)
Java Island
MD62
Flores Island
Banda Sea
MD76
MD25
MD70 (?)
GeoB10053-7
MD65
MD78 (?)
MD28
Lynch's Crater
less rain/ δ18OSW-IVC ↑
more rain/ δ18OSW-IVC ↓
Hypothetical precipitation boundary
Indo-Pacific Warm Pool
Latitude
Longitude
20° N
10° N
0
10° S
20° S
100° E
110° E
120° E
130° E
140° E
150° E
160° E
170° E
180°
60° E
90° E
120° E
150° E
28
28.5
29
27.5
26.5
26
25.5
27

Fig. 6